Chinese Chemical Letters 33 (2022) 2105–2110

Contents lists available at ScienceDirect

Chinese Chemical Letters

journal homepage: www.elsevier.com/locate/cclet

Efficient removal of tetracycline by H_2O_2 activated with iron-doped biochar: Performance, mechanism, and degradation pathways

Xiang Li[a,*], Yan Jia[a], Jiajia Zhang[a], Yang Qin[a], Yijia Wu[a], Minghua Zhou[b,*], Jianhui Sun[a]

[a] School of Environment, Henan Normal University, Key Laboratory of Yellow River and Huai River Water Environment and Pollution Control, Ministry of Education, Henan Key Laboratory for Environmental Pollution Control, International Joint Laboratory on Key Techniques in Water Treatment, Henan Province, Henan Engineering Laboratory of Environmental Functional Materials and Pollution Control, Xinxiang 453007, China
[b] Key Laboratory of Pollution Process and Environmental Criteria, Ministry of Education, Tianjin Key Laboratory of Environmental Technology for Complex Trans-Media Pollution, Tianjin Advanced Water Treatment Technology International Joint Research Center, College of Environmental Science and Engineering, Nankai University, Tianjin 300350, China

ARTICLE INFO

Article history:
Received 3 June 2021
Revised 10 July 2021
Accepted 9 August 2021
Available online 16 August 2021

Keywords:
Fe-BC
Fenton-like
Tetracycline
Removal mechanisms
Degradation pathways

ABSTRACT

In this study, novel iron-doped biochar (Fe-BC) was produced using a simple method, and it was used as an H_2O_2 activator for tetracycline (TC) degradation. Generally, iron loading can improve the separation performance and reactivity of biochar (BC). In the Fe-BC/H_2O_2 system, 92% of the TC was removed within 30 min with the apparent rate constant (k_{obs}) of 0.155 min^{-1}, which was 23.85 times that in the case of the BC/H_2O_2 system (0.0065 min^{-1}). The effects of the H_2O_2 and Fe-BC dosage, initial pH, and TC concentration on the TC removal were investigated. The radical quenching and electron paramagnetic resonance (EPR) measurements demonstrated that the removal of TC using the Fe-BC/H_2O_2 process involved both radical ($^{\bullet}OH$ and $O_2^{-\bullet}$) and non-radical pathways ($^1O_2$ and electron transfer). In addition, the performance of the catalyst was also affected by the persistent free radicals (PFRs) and defective sites on the catalyst. Moreover, the degradation pathways of TC were proposed according to the intermediate products detected by LC-MS and the ecotoxicity of intermediates was evaluated. Finally, the Fe-BC/H_2O_2 showed high resistance to inorganic anions and natural organic matter in aquatic environments. Overall, Fe-BC is expected to be an economic and highly efficient heterogeneous Fenton catalyst for removing the organic contaminants in wastewater.

Recently, antibiotics have been widely used to control infectious diseases and their presence in the environment has aroused dramatic attention, since surface water, groundwater, and even drinking water are contaminated with antibiotics residues [1]. As a general consensus, the existence of antibiotics leads to the development of antibiotic-resistant pathogens that pose a potential threat to ecosystems function and human health [2]. As a broad-spectrum bacteriostatic agent, tetracycline (TC) is widely used in the livestock and aquaculture industry [3]. However, due to the strong bacterial resistance, TC could not be efficiently degraded by traditional methods of wastewater treatment [4]. Therefore, it is necessary to exploit a new process that can effectively degrade it.

Advanced oxidation processes (AOPs) have been exploited to degrade the existing refractory organics in wastewater due to their remarkable treatment effects [5]. AOPs are based on the formation of hydroxyl radicals ($^{\bullet}OH$) in situ, which have high redox potential (2.7 eV) and non-selectivity. In addition, they can oxidize most organic pollutants. Recently, several AOPs, such as O_3 [6], ultraviolet [7], ultrasound [8], Fenton [9], and electro-Fenton processes [10], have been applied to degrade organic contaminants from wastewater. However, these approaches have various drawbacks, such as high cost and energy consumption (O_3, ultraviolet, ultrasound, and electro-Fenton), the need for pH adjustment (Fenton and electro-Fenton), and sludge generation (Fenton). Recently, heterogeneous Fenton-like process becomes a promising choice to overcome the disadvantages of traditional AOPs (massive iron sludge and incapable catalyst recovery) [11].

At present, carbon-based materials have been widely used as catalysts for environmental remediation [12-14]. Specifically, activated carbons (ACs) [15], graphene [16], carbon aerogels [17,18], g-C_3N_4-based materials [19-21], and biochars (BCs) [22], have attracted more and more attentions as H_2O_2 activators. BCs, which are produced from agricultural and industrial waste through the direct thermal decomposition of biomass under anaerobic con-

* Corresponding authors.
E-mail addresses: lixiang2019@htu.edu.cn (X. Li), zhoumh@nankai.edu.cn (M. Zhou).

https://doi.org/10.1016/j.cclet.2021.08.054
1001-8417/

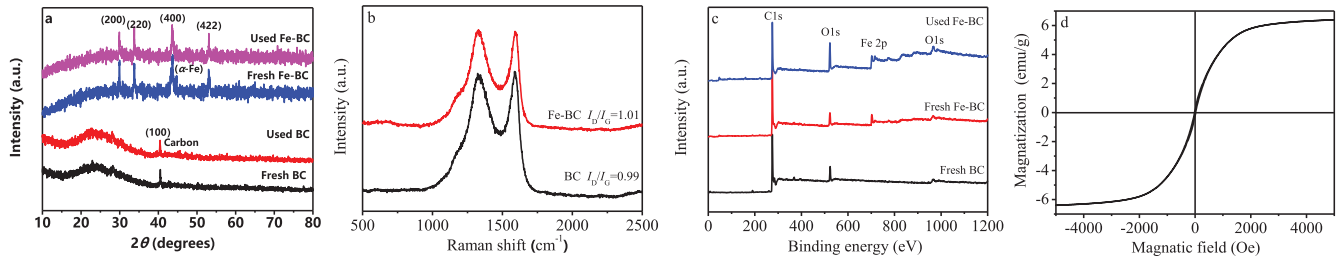

Fig 1. XRD patterns of BC and Fe-BC before and after reaction (a), Raman spectra (b) and XPS survey of BC, Fe-BC and used Fe-BC (c), and magnetic hysteresis loops of Fe-BC (d).

ditions, could be used as substitutes for expensive carbon-based materials. Although BCs have large specific surface areas, multiple pores, abundant active functional groups, and a stable structure, the catalytic performance of original BCs is unsatisfactory. For instance, only 33.3% sulfamethoxazole could be removed by BC/H_2O_2 system, which was much lower than that of by Schwertmannite@BC/H_2O_2 system (100%) under the same conditions [23]. Additionally, the original BCs are difficult to separate. Metal loadings (Fe and Co) not only enhance the catalytic performance of BCs, but they also effectively solve the problem of catalyst recyclability. As Fe spices are non-toxic, relatively inexpensive, and magnetic, they were chosen as metal loads on BCs. Recently, Fe-BC, as an activator for H_2O_2, has aroused widespread attention in removing organic contaminants [24]. The Fe phases loaded on BC has an important effect on the structure and reactivity of Fe-BC. Meanwhile, the contribution of each component in Fe-BC to contaminant degradation was also different. However, only few studies have focused on the performance of Fe additions and the Fe-BC catalytic mechanisms for removing pollutants, especially the generation of by-products and their toxicities in Fe-BC/H_2O_2 process. Therefore, a thorough investigation of Fe-BC as the catalyst to activate H_2O_2 for the removal of TC from water is needed, which can guide the application of Fe-BC/H_2O_2 process in wastewater treatment.

In this study, hydrothermal-pyrolysis, which can uniformly load iron on BC [25], was used to prepare a new Fe-BC composite using wheat stalk and $FeSO_4·7H_2O$ as precursors, and a Fe-BC/H_2O_2 system was proposed to treat tetracycline (TC). The effects of catalyst and H_2O_2 dosage, initial pH, pollutant concentration, and the water matrix on the wastewater treatment were studied. Meanwhile, the reusability of Fe-BC was also studied. Additionally, the catalytic mechanisms of the Fe-BC/H_2O_2 process were studied through the characterization analysis of materials, electron paramagnetic resonance (EPR) detection, chemical quenching experiments, and H_2O_2 consumption detection. Moreover, the degradation products of TC were determined and the possible degradation pathways were speculated. Additionally, the ecotoxicities of TC and its intermediates were evaluated. The characterization details of Fe-BC and the experimental procedures are provided in Supporting information.

The morphology of BC-based materials were detected by scanning electron microscopy (SEM) (Fig. S1 in Supporting information). The BCs retained the irregular flaky structure of the wheat straw with slight surface protrusions. By comparing Figs. S1a and b, it can be seen that there is no obvious difference in the surface morphology of BC before and after the reaction, indicating that BC alone has no or little effect on the TC pollutants. A large number of tiny particles could be clearly seen attached to the Fe-BC surface. These particles are known to be loaded with iron or iron oxide based on the element distribution. These structures provided more specific surface areas and active sites which can in favor of enhancing catalytic activity, compared to original BCs (Table S3 and Figs. S2a in Supporting information). Compared with Figs. S1c and d, it was noticed that the particles attached to the Fe-BC surface before and after the reaction had significantly changed and the particles became coarser and tended to aggregate after the reaction, indicating that the Fe loaded on the BC played an important role in the reaction process. The microstructure and compositional distribution of the BC and Fe-BC were further investigated using transmission electronic microscopy (TEM), energy dispersive X-ray detector (EDX), and EDX-mapping. The TEM image (Fig. S3a in Supporting information) showed that Fe was uniformly and densely doped on the surface of Fe-BC, which is in agreement with the SEM results. The distribution of the C, O, and Fe components on the surface of the materials was determined using EDX-mapping. As presented in Figs. S3b and c and Fig. S4 (Supporting information), compared with the pristine BC sample, the Fe content of the Fe-BC sample was significantly increased.

In Fig. 1a, the XRD patterns of the prepared BC and Fe-BC before and after the reaction clearly demonstrated the structures and changes of these materials. The broadened peaks cantered at $2\theta = 23°$ and 42.2° were found in BC before and after the reaction, corresponding to the (002) and (100) planes of crystalline carbon, respectively [26]. The apparent peaks at $2\theta = 33.24°$, 43.28° and 53.73° (JCPDS No. 19-0629) in the fresh and used Fe-BC were assigned to the (220), (400) and (422) crystal planes of magnetite [25]. Moreover, the $2\theta = 30.1°$ and 44.8° might have been corresponded to γ-Fe_3O_4 and α-Fe, respectively [27]. The XRD patterns demonstrated that Fe was successfully loaded on the BC surface, which is in agreement with the SEM results. The positions of the diffraction peaks were almost unchanged before and after the reaction, illustrating that the crystal structures of the material were relatively stable. The diffraction peak intensity of the iron species changed, showing that Fe played a key role in the degradation of TC.

Raman spectroscopy was applied to further uncover the crystallization and the defect degree on the catalysts surface, as described in Fig. 1b. The D band (~1350 cm^{-1}) was ascribed to the disordered graphitic carbon or amorphous carbon, and the G band (~1580 cm^{-1}) was attributed to the sp^2-hybridised graphitic carbon [28]. The carbon-based material defects could be expressed using the relative intensity ratio of I_D/I_G. It could be inferred from the Raman spectra that the I_D/I_G of BC was 0.99 and that of Fe-BC was 1.01, indicating that Fe-BC formed more defects in the generation process [29].

X-ray photoelectron spectroscopy (XPS) measurements were conducted to probe the surface element composition and valence state data. As illustrated in Fig. 1c, the survey spectra of XPS described the presence of C and O for both BC and Fe-BC samples. The peak at 708.8 eV (Fe 2p) was observed for Fe-BC, which is in agreement with the results of EDX-mapping and XRD, suggesting that Fe was successfully loaded onto the BC surface in the form of Fe^0, Fe^{2+}, and Fe^{3+}. In addition, we found that the O content of used Fe-BC was higher than that of fresh Fe-BC, indicating oxygen-containing functional groups play an important

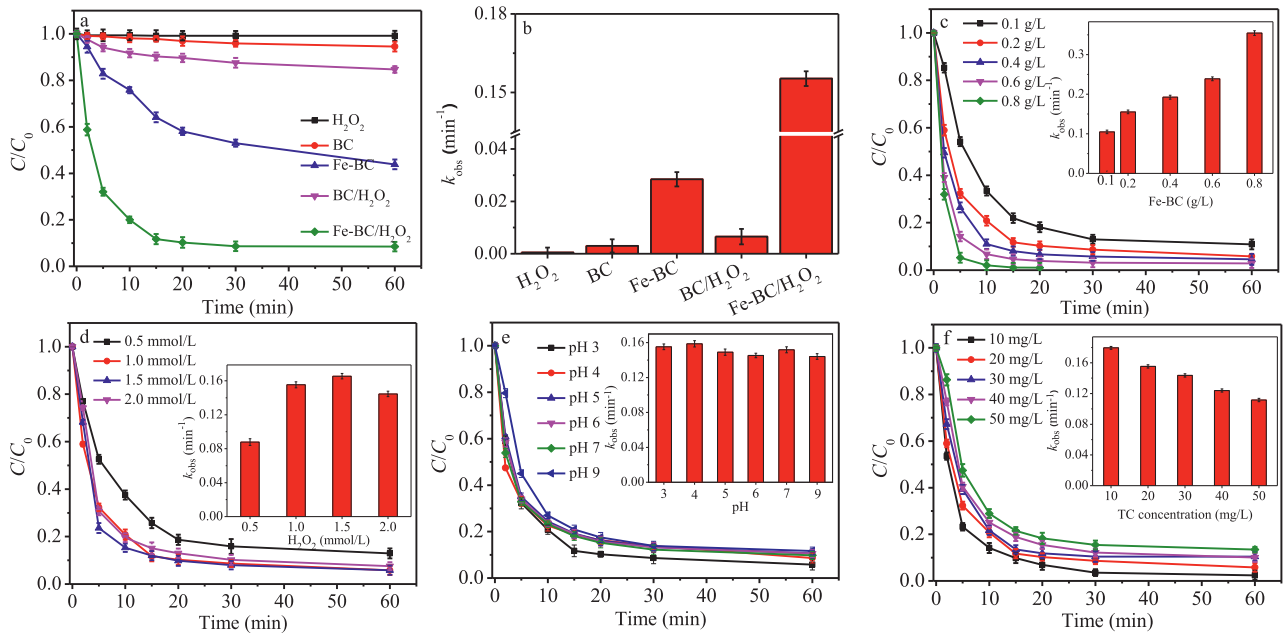

Fig 2. Influence of different system (a and b), Fe-BC dosage (c), H_2O_2 concentration (d), initial pH values (e), and initial TC concentration (f) on the TC removal using the Fe-BC/H_2O_2 system. Reaction conditions: [TC] = 20 mg/L, [H_2O_2] = 1 mmol/L, [Fe-BC] = 0.2 g/L, and initial pH 3.

role in removal of TC, which also discussed in the following results.

The magnetic hysteresis loops in Fig. 1d reflect the magnetization properties of Fe-BC. The small coercivity indicates that Fe-BC is a soft magnetic material, and the small remanence indicate that Fe-BC is a typical superparamagnetic material. Moreover, Fe-BC had a high saturation magnetization value of about 6.2 emu/g, indicating that it was easily attracted to external magnets and that it could be easily separated from the system after the reaction.

The catalytic performance of materials was estimated and the results were shown in Figs. 2a and b. Less than 1% TC was eliminated only in the H_2O_2 system, indicating that H_2O_2 can hardly degrade TC effectively in the absence of external catalysis. The removal efficiency of TC was 5.4% by BC within 60 min, illustrating that BC can remove a part of TC due to its porous structure. The removal efficiency of TC was 15.3% in the BC/H_2O_2 process, confirming that BC can promote the decomposition of H_2O_2 [30]. In addition, 56% TC was removed by Fe-BC alone in 60 min. The TC removal may have been caused by adsorption (N_2 adsorption-desorption isotherm results in Fig. S2 in Supporting information) and the micro-electrolysis because of the existence of Fe species (Fe^0) on Fe-BC surface (XRD and XPS results). In the Fe-BC/H_2O_2 process, ~92% of TC was removed, so it can be inferred that Fe plays a key role in TC removal. The k_{obs} of the Fe-BC/H_2O_2 process was 0.155 min^{-1}, which is 23.85 times higher than that of the BC/H_2O_2 process (0.0065 min^{-1}), indicating that Fe doping endowed the material with higher adsorption and reactivity.

Fig. 2c shows the influence of the Fe-BC dosage on the TC removal. The removal efficiency of TC increased with the increase of Fe-BC dosage. 89% of the TC was removed within 60 min under the condition of 0.1 g/L Fe-BC. When the Fe-BC dosage was 0.2 g/L, 94.2% of TC could be removed. The dosage of Fe-BC was further increased to 0.6 g/L and 0.8 g/L, a similar removal efficiency was obtained within only 10 min and 5 min, respectively. The k_{obs} of the Fe-BC/H_2O_2 process increased with the increase of the Fe-BC dosage from 0.105 min^{-1} of 0.1 g/L to 0.355 min^{-1} of 0.8 g/L. These results indicate that increasing the dose of Fe-BC can provide more active sites.

The H_2O_2 concentration effect on the TC removal is shown in Fig. 2d. 87% of TC was removed within 60 min with 0.5 mmol/L H_2O_2. When the H_2O_2 increased to 1.0 mmol/L, the removal efficiency of TC reached 94.2% within 60 min. However, with a further increase in H_2O_2 (1.5 and 2.0 mmol/L), the removal of TC was not further enhanced, corresponding to the trend of k_{obs} (0.088, 0.155, 0.165 and 0.145 min^{-1}). One possible for the results was that the excess H_2O_2 in the process consumed $^{\bullet}OH$ according to Eq. 1 [5].

$$H_2O_2 + {}^{\bullet}OH \rightarrow H_2O + HO_2{}^{\bullet} \quad (1)$$

pH is usually considered as a critical factor that affects heterogeneous Fenton reactions. In addition, TC is an amphoteric molecule with multiple pK_a and appeared in different chemical state at different pH values [31]. Therefore, the TC removal using the Fe-BC/H_2O_2 process at different initial pH values (3.0-9.0) was evaluated. As exhibited in Fig. 2e, TC could be effectively removed at pH of 3.0-4.0. while the removal efficiency of TC slightly decreased from 91.37% to 88.37% with increasing pH from 4.0 to 9.0 under experimental conditions, which is consist with previous report [32]. Similarly, the values of k_{obs} vary with pH, which are 0.155, 0.159, 0.149, 0.145, 0.151, and 0.144 min^{-1} at pH 3.0-9.0. The reasons why TC can be effectively removed under neutral or alkaline conditions are explained as follows: TC present different forms under different pH value, *i.e.*, cationic (pH < 3.3), zwitterionic (3.3 < pH < 7.7), and anionic species (pH > 7.7). When pH > 3.3, TC mainly exists in the form of zwitterionic ($TCH_2{}^0$) and anions (TC^-), which are vulnerable to attack by reactive oxygen species (ROS) due to the higher electronic density in the ring system. In addition, previous study found that H_2O_2 could directly attack TC molecules to form hydroxyl or to remove certain groups to achieve TC removal under alkaline conditions [33].

The TC concentration is also an important factor for pollutants removal. As shown in Fig. 2f, at a concentration of 10 mg/L, 90% TC could be removed in 15 min and 98% in 60 min. As the TC concentration increased to 20, 30, 40 and 50 mg/L, the degradation rates correspondingly decreased to 94%, 91%, 90%, and 87%, respectively. The quantity of the produced free radicals and active sites in the Fe-BC/H_2O_2 process was limited and could not respond to the excessive amount of TC. Therefore, the k_{obs} decreased with the increase in the TC concentration.

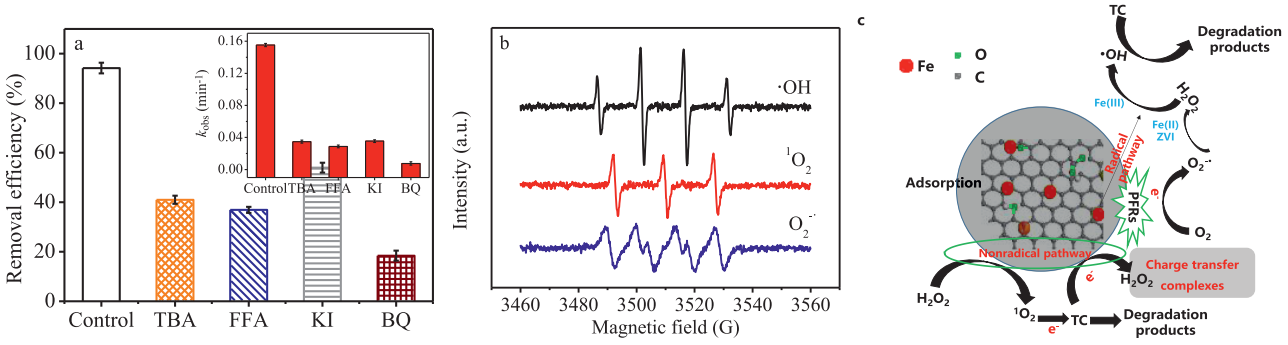

Fig 3. Influence of different scavengers on the removal efficiency of TC (a), the EPR spectra of the Fe-BC/H_2O_2 process with DMPO and TEMP (b), and the possible activate mechanism of the TC removal using the Fe-BC/H_2O_2 process (c). Reaction conditions: [TC] = 20 mg/L, [H_2O_2] = 1.0 mmol/L, [Fe-BC] = 0.2 g/L, [TBA]$_0$ = 100 mmol/L, [BQ]$_0$ = [FFA]$_0$ = [KI]$_0$ = 20 mmol/L, [DMPO]$_0$ = [TEMP]$_0$ = 10 mmol/L, and initial pH 3.

Based on previous experience, it was predicted that the free radical and non-free radical pathways are the main causes of TC removal using the Fe-BC/H_2O_2 process [34]. Therefore, quenching experiments were executed to confirm the reaction mechanism. The results of the quenching experiments are shown in Fig. 3a. First, the role of the free radicals was discussed, and tert-butyl alcohol (TBA) was applied to quench ·OH with rate constants of 4.8-7.6 × 10^8 L mol^{-1} s^{-1} [35]. The removal efficiency of TC decreased from 94% to 41% within 60 min after adding TBA, thus confirming the formation of ·OH in the Fe-BC/H_2O_2 process. The production of ·OH in the Fenton reaction is generally considered to be the reaction of Fe^{2+} with H_2O_2. Additionally, *p*-benzo-quinone (*p*-BQ) was chosen to scavenge $O_2^{-\cdot}$ (k = 0.9-1.0 × 10^9 L mol^{-1} s^{-1}) [36]. The TC degradation effects were significantly affected, from 94% to 18% in 60 min, and the k_{obs} decreased from 0.155 min^{-1} to 0.008 min^{-1} after the addition of *p*-BQ. This indicated that $O_2^{-\cdot}$ played a pivotal role in the TC removal in the Fe-BC/H_2O_2 process. The generation of $O_2^{-\cdot}$ came from the reaction of Fe^{2+}/Fe^{3+} with O_2 Eqs. 2 and 3.

$$Fe^{2+} + O_2 \rightarrow Fe^{3+} + O_2^{-\bullet} \quad (2)$$

$$H_2O_2 + Fe^{3+} + 2OH^- \rightarrow Fe^{2+} + O_2^{-\bullet} + 2H_2O \quad (3)$$

As for the non-free radical pathway, furfuryl alcohol (FFA) was considered to be the quenching agent for $^1O_2$, which was used in this study to confirm the existence of $^1O_2$ (k = 1.2 × 10^8 L mol^{-1} s^{-1}) [37]. The removal efficiency of TC ranged from 94% to 36% with the presence of FFA, with the k_{obs} ranging from 0.155 min^{-1} to 0.029 min^{-1}, suggesting that the TC removal was significantly inhibited. In the Fe-BC/H_2O_2 process, $^1O_2$ was generated, as shown in Eqs. 4-6 [38]. Potassium iodide (KI) quenched ROS on the material surfaces [39], and the TC removal efficiency decreased from 94% to 54% after adding KI. It was proven that the Fe-BC surface bound some ROS, which was crucial in the reaction.

$$O_2^{-\bullet} + H_2O_2 \rightarrow {}^1O_2 + OH^- + {}^\bullet OH \quad (4)$$

$$2H_2O_2 \rightarrow {}^1O_2 + 2H_2O \quad (5)$$

$$2O_2^{-\bullet} + 2H^+ \rightarrow {}^1O_2 + H_2O_2 \quad (6)$$

EPR was also measured and used to validate the TC degradation pathway, and the results are demonstrated in Fig. 3b. In the tests, 5,5-dimethyl-1-pyrroline N-oxide (DMPO) and 2,2,6,6-tetramethyl-4-piperidinol (TEMP) were applied to capture radicals. When captured with DMPO, typical DMPO-OH signals were clearly identified, indicating the generation of ·OH in Fe-BC/H_2O_2 process. Also, DMPO was a spin trapping agent for $O_2^{-\cdot}$. With the assistance of DMPO, representative quartet characteristic EPR signals appeared, corresponding to the production of $O_2^{-\cdot}$. Additionally, $^1O_2$ was trapped by TEMP, through which the triplet EPR spectrum (1:1:1) was detected and attributed to signals for TEMP-$^1O_2$, thus implying the generation of $^1O_2$. These results clearly confirmed that the removal of contaminants in the Fe-BC/H_2O_2 process involved free radical and non-free radical pathways, which is in agreement with the quenching results. To further clarify the role of iron species and H_2O_2 in Fe-BC/H_2O_2 system, the ROS formed in Fe-BC and BC/H_2O_2 process were also detected by EPR and the results showed that the presence of iron species and H_2O_2 facilitated the production of $O_2^{-\cdot}$ and $^1O_2$ (the details were shown in Fig. S5 in Supporting Information). Moreover, the H_2O_2 consumption and Fe^{2+} dissolution in the Fe-BC/H_2O_2 process further demonstrates that non-free radical pathways exist (Fig. S6 in Supporting information).

In order to understand components transformation on the surface of Fe-BC, the used Fe-BC were characterized by EDX, Raman, XPS, and FTIR and the results were displayed in Fig. S7 (Supporting information). The EDX spectra of used Fe-BC were showed in Fig. S7a and Table S2 (Supporting information). Compared with the fresh Fe-BC, the Fe contents on the surface of the used Fe-BC decreased from 27.96% to 18.65% while the O content increased from 14.15% to 23.56%, illustrating that a part of Fe was dissolved and oxidized during the reaction and that Fe plays a key role in the TC removal. Raman spectra were also obtained to further understand the changes of crystallization and defects of the catalysts after reaction. Fig. S7b showed that The Fe-BC defects changed after the reaction, and the I_D/I_G of the used Fe-BC decreased from 1.01 to 0.98, which might have been caused by the damage of the defective edges, the change of the functional groups, and the interactions between the adsorbed pollutants and sp^2 hybrid carbon system [40]. Thus, the defective sites of Fe-BC took part in the degradation of TC. The high-resolution C 1s O 1s, and Fe 2p XPS spectra were presented in the Figs. S7c-e. The XPS spectra of C 1s were divided to four peaks (Fig. S7c) at around 288.5, 286.7, 285.6, and 284.7 eV, corresponding to C=O/C=N, C−O−C, C−OH/C−N and C−C/C=C, respectively [41]. The spectra of O 1s were divided into three peaks (Fig. S7d) at 533, 530.7 and 529.9 eV, corresponding to C=O, C−OH and Fe−O, respectively [42]. Interestingly, it was found that C=O increased and that C−OH decreased in both the C 1s and O 1s XPS spectra after the reaction, suggesting that C=O might play a catalytic role in the Fe-BC/H_2O_2 process [43]. The Fe 2p spectra were resolved to a variety of states of iron species (Fe^{3+}, Fe^{2+} and Fe^0) (Fig. S7e). Notably, the amounts of Fe^0 of Fe-BC decreased, while Fe^{2+} and Fe^{3+} increased after the reaction, demonstrating that Fe^0 was oxidized. FTIR technology was used to distinguish the functional groups of BC-based materials. Fig. S7f shows the FTIR spectra of Fe-BC before and after the reaction. The broad absorption peak appearing at 3426 cm^{-1} is ascribed to the stretching vibrations of the −OH groups: 2930, 1588, 1103 and 807

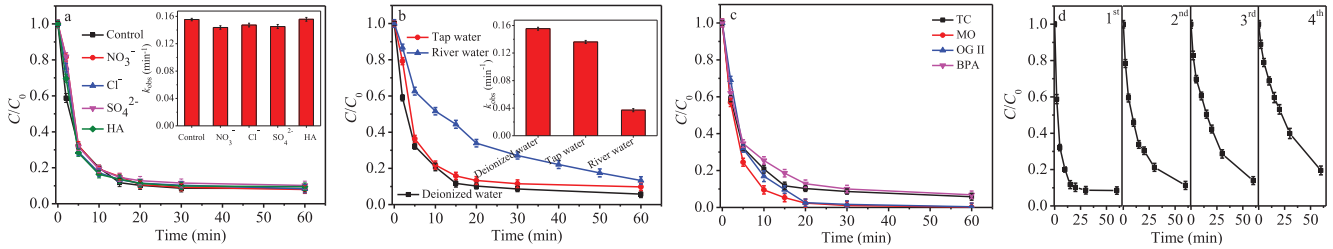

Fig 4. Influence of inorganic ions and HA on TC removal by the Fe-BC/H_2O_2 process (a), TC removal in deionized water, tap water, and river water (b), the removal of different contaminants in the Fe-BC/H_2O_2 system (c), and the reusability of Fe-BC on removal of TC (d). Reaction conditions: [TC]= 20 mg/L, [H_2O_2] = 1.0 mmol/L, [Fe-BC] = 0.2 g/L, [NO_3^-]$_0$ = [Cl^-]$_0$ = [SO_4^{2-}]$_0$ = 20 mmol/L, [HA]$_0$ = 10 mg/L, and initial pH 3.

cm^{-1} to $-CH_2$, C=C, C−O and C−H, respectively [44]. The absorption peak at 550 cm^{-1} is probably associated with the Fe-O bond stretching vibrations of Fe_3O_4 nanoparticles [45], or possibly the binding of iron adhering to the surface of Fe-BC with the oxygen-containing functional groups [46]. It should be noted that the band of C=C and Fe−O slightly diminished, confirming that C=C and Fe−O provided active sites for the TC removal. These results are consistent with the XPS results.

On the basis of above results, the possible reaction mechanisms for the pollutants removal by the Fe-BC/H_2O_2 process were put forward, as shown in Fig. 3c. The TC removal was primarily related to the adsorption and oxidative degradation (the species distribution of TC on Fe-BC were shown in Fig. S8 in Supporting Information). First, the TC was adsorbed on the surface of Fe-BC, then H_2O_2 is activated by Fe-BC to produce ROS, and finally the adsorbed TC was *in situ* attacked by ROS. The oxidative degradation mainly included two pathways (radical pathway and non-radical pathway). The iron species on the Fe-BC surface could activate O_2 and H_2O_2 to generate $O_2^{-\bullet}$ and $^\bullet$OH. Meanwhile, H_2O_2 reacted with C−OH to form $^\bullet$OH and $HO_2^\bullet$. These free radicals could rapidly oxidize and decompose pollutants. It was found that persistent free radicals (PFRs) were produced during the BC pyrolysis, and the PFRs existence was confirmed using EPR spectroscopy (Fig. S9 in Supporting information). The PFRs in the BC could directly activate H_2O_2 to generate $^\bullet$OH, and they could also transfer electrons to the oxygen molecules to form $O_2^{-\bullet}$, as described in a previous work [22]. Additionally, H_2O_2 was decomposed to produce $^1O_2$ (Eq. 4), which could remove pollutants using electron transfer. Furthermore, Fe-BC provided electrons primarily via a graphite electron donor-transfer complex in the BC and directly transferred electrons to the H_2O_2 as an electronic shuttle. The combination of radical and non-radical processes could degrade the organic contaminants.

The degradation intermediates of TC were identified using LC-MS. Base on the transformation intermediates identified in the present work and previous research [47], three possible degradation pathways of TC in the Fe-BC/H_2O_2 process were illustrated in Fig. S10 (Supporting information). Pathway I: product **P1** (*m/z* 417) was generated by *N*-demethylation of TC attacked by ROS, the amino group of **P1** was destroyed to form *P2* (*m/z* 376), and the benzene ring and amino group of **P2** were attacked by ROS to form **P3** (*m/z* 339), which then removed −OH and methylates to form **P4** (*m/z* 309), Then, P4 was further broken into P5 (*m/z* 287) under the attack of ROS. The similar mechanisms have been reported in previous work [47]. Pathway II: Due to the active substance presented, the deamidation reaction of TC could occur, resulting in the loss of dimethylamino group to form **P6** (*m/z* 362) [48]. Subsequently, P6 underwent the opening of ring to form **P7** (*m/z* 274). Pathway III: TC could be converted into **P8** (*m/z* 461) by hydroxylation [49], and then the C=C on **P8** was oxidized by ROS to generate hydroxyl and ketone groups, forming **P9** (*m/z* 477). As the reaction proceeds, these intermediates formed by the above three pathways were further degraded into small molecular weight organics, such as **P10** (*m/z* 242) and P12 (*m/z* 218), then they were further decomposed into the smaller molecules **P11** (*m/z* 114), **P13** (*m/z* 118), P14 (*m/z* 60), P15 (*m/z* 90)) under the action of ROS. Finally, the intermediates were eventually oxidized to CO_2, H_2O, and NH_4^+. In addition, the acute toxicity (represented by oral rat LD_{50}) and mutagenicity of intermediates were predicted by the quantitative structure-activity relationship (QSAR) method using the Toxicity Estimation Software Tool (T.E.S.T.) (Fig. S11 in Supporting information)

Inorganic anions, *e.g.*, Cl^-, NO_3^-, and SO_4^{2-}, and natural organic matter (humic acid, HA) are usual water ingredients in the actual water. To estimate the influence of inorganic anions on the Fe-BC/H_2O_2 process, 20 mmol/L of Cl^-, NO_3^-, and SO_4^{2-} were added into the process, and compared with control experiment. As depicted in Fig. 4a, negligible effects on the 60 min removal were obtained in the presence of these matrices. However, when NO_3^-, Cl^- and SO_4^{2-} were added, the obtain k_{obs} values (0.144, 0.147 and 0.145 min^{-1}) were slightly decreased compared to the control, presumably due to the clearing of a small amount of reactive radicals as exhibited in Eqs. 7-9 [50-52]. Moreover, HA can promote the degradation of TC to some extent, the k_{obs} value was 0.156 min^{-1}, which might be ascribed to the fact that HA could expedite circulation of iron and enhance the pollutants elimination [53]. In addition, HA can act as a catalyst to activate H_2O_2 to form ROS therefore promoting the degradation performance [54]. In conclusion, these results suggested that Fe-BC in this study could achieve excellent results for TC removal in practical water treatment.

$$Cl^- + {}^\bullet OH \rightarrow ClOH^{-\bullet} \quad (7)$$

$$NO_3^- + {}^\bullet OH \rightarrow NO_3^{-\bullet} + OH^- \quad (8)$$

$$SO_4^{2-} + {}^\bullet OH \rightarrow SO_4^{-\bullet} + OH^- \quad (9)$$

To further investigate the practicability of the prepared Fe-BC catalyst in removing TC pollutants from real aquatic systems, the catalytic degradation reactions were carried out in different water processes. As demonstrated in Fig. 4b, the removal efficiencies of TC were 90.3% and 86.7% within 60 min in tap water and river water, respectively, and the corresponding values of k_{obs} were 0.136 and 0.037 min^{-1}. Compared to deionized water (94.2% and 0.155 min^{-1}), the removal efficiency and rate constant of TC were inhibited in river water. The reason might be that the coexisting ions and organic matters in the river water would consume ROS [41]. As we all know, there are some organic pollutants in the nature water bodies, such as azo dyes and endocrine disruptors. To prove the feasibility of Fe-BC for other organic pollutants, the degradations of methyl orange (MO), orange II (OGII), and bisphenol A (BPA) were studied. Fig. 4c showed that the removal efficiencies of these organic pollutants reached more than 90%. These results indicated that Fe-BC had a great prospect in actual wastewater treatment.

Reusability of catalysts plays a significant role in practical application. To test the reusability performance of Fe-BC in this study,

the catalysts were recovered by magnetic separation, and washed several times with ultrapure water, then directly put into the next cycle. As illustrated in Fig. 4d, the removal efficiency of Fe-BC gradually decreased as the number of cycles increased, probably because the pore structure of the catalyst was blocked by contaminants or the active sites were occupied, which was consist with the results of N_2 adsorption-desorption isotherms of the used Fe-BC. Even so, the degradation effect of the fourth time still reached 80.5% at 60 min, which indicated that Fe-BC is promising for practical wastewater treatment. In addition, the magnetic separation property of Fe-BC is shown in Fig. S12 (Supporting information). As depicted, Fe-BC showed a great magnetic response when a permanent magnet was nearby, indicating the Fe-BC catalyst was recyclable, which helped to avoid secondary pollution.

Fe-BC catalysts were successfully fabricated using a simple and effective method in this work. The obtained Fe-BC displayed outstanding activation performance for the H_2O_2 in TC removal, which was improved with a moderate increase in Fe-BC and in the H_2O_2 dosage (favored at acidic condition). The EPR and quenching experiments verified that the TC removal mechanisms by the Fe-BC/H_2O_2 process depended on both radical ($^{\bullet}OH$ and $O_2^{-\bullet}$) and non-radical pathways ($^1O_2$ and electron transfer). Moreover, the defective sites and PFRs on the catalysts facilitate the removal of TC. The degradation mechanisms of TC by Fe-BC/H_2O_2 process were proposed based on above results. Based on the identified intermediate products, the possible reaction pathways of TC were proposed. Furthermore, the ecotoxicity of TC and degradation intermediates were estimated and the acute toxicity of most intermediates was much lower than that of TC. Finally, the Fe-BC showed remarkable reusability and the adaptability for removal of TC in real samples (river water and tap water).

Declaration of competing interest

The authors declare that they have no known competing financial interests or personal relationships that could have appeared to influence the work reported in this paper.

Acknowledgments

This work was supported by National Natural Science Foundation of China (No. 21906045), The 2020 Scientific Research Project for Postgraduates of Henan Normal University (No. YL202029).

Supplementary materials

Supplementary material associated with this article can be found, in the online version, at doi:10.1016/j.cclet.2021.08.054.

References

[1] Q. Wang, Q. Xue, T. Chen, et al., Chin. Chem. Lett. 32 (2021) 609–619.
[2] J. Cao, Z. Xiong, B. Lai, Chem. Eng. J. 343 (2018) 492–499.
[3] D. Zhang, Q. He, X. Hu, et al., Colloid. Surf. A: Physicochem. Eng. Asp. (2021) 615.
[4] Z. He, X. Wang, Y. Luo, et al., Chemosphere 277 (2021) 130327.
[5] X. Li, M. Zhou, Y. Pan, Chemosphere 212 (2018) 853–862.
[6] P. Ormad, S. Cortes, A. Puig, J.L. Ovelleiro, Water Res. 31 (1997) 2387–2391.
[7] A. Zuorro, M. Fidaleo, M. Fidaleo, R. Lavecchia, J. Environ. Manage. 133 (2014) 302–308.
[8] T. Huang, G.M. Zhang, S. Chong, et al., Ultrason. Sonochem. 37 (2017) 676–685.
[9] X.L. Hao, L.Y. Zou, G.S. Zhang, Y.B. Zhang, Chin. Chem. Lett. 20 (2009) 99–101.
[10] J. Li, Y. Li, Z. Xiong, et al., Chin. Chem. Lett. 30 (2019) 2139–2146.
[11] X. Li, M. Zhou, Y. Pan, J. Hazard. Mater. 353 (2018) 454–465.
[12] L. Fu, R. Wang, C. Zhao, et al., Chem. Eng. J. 414 (2021) 128857.
[13] H. Yang, C. He, L. Fu, et al. , Chin. Chem. Lett. 32 (2021) 3202–3206.
[14] R. Wang, C. He, W. Chen, et al. , Chin. Chem. Lett. 32 (2021) 3821–3824.
[15] V.P. Santos, M.F.R. Pereira, P.C.C. Faria, J.J.M. Órfão, J. Hazard. Mater. 162 (2009) 736–742.
[16] Q. Wang, H. Li, J. Yang, et al., Appl. Catal. B: Environ. 192 (2016) 182–192.
[17] M. Liu, Z. Feng, X. Luan, et al., Environ. Sci. Technol. 55 (2021) 6042–6051.
[18] F. Xiao, Z. Wang, J. Fan, et al., Angew. Chem. Int. Ed. 60 (2021) 10375–10383.
[19] B. Li, L. Nengzi, R. Guo, et al., Chin. Chem. Lett. 31 (2020) 2705–2711.
[20] M. Ding, J. Zhou, H. Yang, et al., Chin. Chem. Lett. 31 (2020) 71–76.
[21] D. Huang, X. Sun, Y. Liu, et al. , Chin. Chem. Lett. 32 (2021) 2787–2791.
[22] X. Zhang, P. Sun, K. Wei, et al., Chem. Eng. J. 385 (2020) 123921.
[23] Z. Yang, P. Zhu, C. Yan, et al., Chemosphere 266 (2021) 129175.
[24] X. Li, Y. Qin, Y. Jia, et al., Chemosphere 274 (2021) 129766.
[25] X. Li, Y. Jia, M. Zhou, et al., J. Hazard. Mater. 397 (2020) 122764.
[26] A.L. Cazetta, T. Zhang, T.L. Silva, et al., Appl. Catal. B: Environ. 225 (2018) 30–39.
[27] Y. Long, Y. Huang, H. Wu, et al., Chem. Eng. J. 369 (2019) 542–552.
[28] A. Shahzad, J. Ali, J. Ifthikar, et al., J. Hazard. Mater. 392 (2020) 122316.
[29] S. Zhu, X. Huang, F. Ma, et al., Environ. Sci. Technol. 52 (2018) 8649–8658.
[30] P. Sun, Y. Li, T. Meng, et al., Water Res. 147 (2018) 91–100.
[31] S. Ma, J. Jing, P. Liu, et al., J. Hazard. Mater. 392 (2020) 122437.
[32] S. Xin, G. Liu, X. Ma, et al., Appl. Catal. B: Environ. 280 (2021) 119386.
[33] Y. Chen, Y. Ma, J. Yang, et al., Chem. Eng. J. 307 (2017) 15–23.
[34] Q. Jin, Z. Chen, Q. Chen, et al., J. Hazard. Mater. 404 (2021) 124142.
[35] Y.-d. Chen, Y.-C. Lin, S.-H. Ho, et al., Bioresour. Technol. 259 (2018) 104–110.
[36] C. Chen, T. Ma, Y. Shang, et al., Appl. Catal. B: Environ. 250 (2019) 382–395.
[37] B.M. Peterson, A.M. McNally, R.M. Cory, et al., Environ. Sci. Technol. 46 (2012) 7222–7229.
[38] T. Jedsukontorn, V. Meeyoo, N. Saito, M. Hunsom, Chin. J. Catal. 37 (2016) 1975–1981.
[39] Z. Huang, H. Bao, Y. Yao, et al., Appl. Catal. B: Environ. 154-155 (2014) 36–43.
[40] Z. Pi, X. Li, D. Wang, et al., J. Clean. Prod. 235 (2019) 1103–1115.
[41] C. Liu, L. Chen, D. Ding, T. Cai, Appl. Catal. B: Environ. 254 (2019) 312–320.
[42] F. Xiao, W. Li, L. Fang, D. Wang, J. Hazard. Mater. 308 (2016) 11–20.
[43] C. Liu, Z. Diao, W. Huo, et al., Environ. Pollut. 239 (2018) 698–705.
[44] Z. Zhao, Y. Cao, S. Li, Y. Zhang, Bioresour. Technol. 320 (2021) 124295.
[45] C.M. Hung, C.P. Huang, C.W. Chen, et al., Environ. Pollut. 265 (2020) 114914.
[46] Z. Li, Y. Sun, Y. Yang, et al., J. Hazard. Mater. 383 (2020) 121240.
[47] S. Yang, Y. Feng, D. Gao, et al., J. Hazard. Mater. 407 (2021) 124361.
[48] Y. Liu, J. Li, L. Wu, et al., Sci. Total Environ. 761 (2021) 143956.
[49] Y. Cao, K. Cui, Y. Chen, et al., Solid State Sci. 113 (2021) 106548.
[50] Z. Zhao, J. Zhao, C. Yang, Chem. Eng. J. 327 (2017) 481–489.
[51] S.P. Mezyk, T.D. Cullen, K.A. Rickman, B.J. Mincher, Int. J. Chem. Kinet. 49 (2017) 635–642.
[52] J. Wang, L. Tang, G. Zeng, et al., Appl. Catal. B: Environ. 209 (2017) 285–294.
[53] X. Huang, X. Hou, F. Jia, et al., ACS Appl. Mater. Inter. 9 (2017) 8751–8758.
[54] B. Yang, X. Cheng, Y. Zhang, et al., J. Hazard. Mater. 407 (2021) 124853.